Astronomy & Astrophysics

LETTER TO THE EDITOR

The strong magnetic field of the large-amplitude β Cephei pulsator V1449 Aquilae[*],[**]

S. Hubrig[1], I. Ilyin[1], M. Briquet[2,3], M. Schöller[4], J. F. González[5], N. Nuñez[5], P. De Cat[6], and T. Morel[7]

[1] Leibniz-Institut für Astrophysik Potsdam (AIP), An der Sternwarte 16, 14482 Potsdam, Germany
e-mail: shubrig@aip.de
[2] Instituut voor Sterrenkunde, Katholieke Universiteit Leuven, Celestijnenlaan 200 D, 3001 Leuven, Belgium
[3] LESIA, Observatoire de Paris, CNRS, UPMC, Université Paris-Diderot, 92195 Meudon, France
[4] European Southern Observatory, Karl-Schwarzschild-Str. 2, 85748 Garching bei München, Germany
[5] Instituto de Ciencias Astronomicas, de la Tierra, y del Espacio (ICATE), 5400 San Juan, Argentina
[6] Koninklijke Sterrenwacht van België, Ringlaan 3, 1180 Brussel, Belgium
[7] Institut d'Astrophysique et de Géophysique, Université de Liège, Allée du 6 Août, Bât. B5c, 4000 Liège, Belgium

ABSTRACT

Aims. Only for very few β Cephei stars has the behaviour of the magnetic field been studied over the rotation cycle. During the past two years we have obtained multi-epoch polarimetric spectra of the β Cephei star V1449 Aql with SOFIN at the Nordic Optical Telescope to search for a rotation period and to constrain the geometry of the magnetic field.
Methods. The mean longitudinal magnetic field is measured at 13 different epochs. The new measurements, together with the previous FORS 1 measurements, have been used for the frequency analysis and the characterization of the magnetic field.
Results. V1449 Aql so far possesses the strongest longitudinal magnetic field of up to 700 G among the β Cephei stars. The resulting periodogram displays three dominant peaks with the highest peak at $f = 0.0720\,\mathrm{d}^{-1}$ corresponding to a period $P = 13\overset{\mathrm{d}}{.}893$. The magnetic field geometry can likely be described by a centred dipole with a polar magnetic field strength B_{d} around 3 kG and an inclination angle β of the magnetic axis to the rotation axis of $76 \pm 4°$. As of today, the strongest longitudinal magnetic fields are detected in the β Cephei stars V1449 Aql and ξ^1 CMa with large radial velocity amplitudes. Their peak-to-peak amplitudes reach $\sim 90\,\mathrm{km\,s}^{-1}$ and $\sim 33\,\mathrm{km\,s}^{-1}$, respectively. Concluding, we briefly discuss the position of the currently known eight magnetic β Cephei and candidate β Cephei stars in the Hertzsprung-Russell (H-R) diagram.

Key words. stars: early-type – stars: rotation – stars: individual: V1449 Aql – stars: magnetic field – stars: oscillations – stars: variables: general

1. Introduction

Before the CoRoT mission, the B1.5 II-III star V1449 Aql (=HD 180642) was known as a β Cephei pulsator with a high-amplitude radial mode of frequency $5.487\,\mathrm{d}^{-1}$ (Waelkens et al. 1998). White light photometry from space revealed the rich frequency spectrum of this target (Degroote et al. 2009) with the first detection of solar-like oscillations in a massive star (Belkacem et al. 2009). Additional ground-based, multi-colour photometry and high-resolution spectroscopy were used to put constraints on the atmospheric parameters and the chemical abundances, and to identify three modes of low amplitudes (Briquet et al. 2009). Notably, the dominant mode does not behave sinusoidally, and the first velocity moment $\langle v^1 \rangle$ has a peak-to-peak amplitude of about 90 km s^{-1}. This is the third largest peak-to-peak radial-velocity amplitude measured among β Cephei stars, after BW Vul (e.g. Crowe & Gillet 1989) and σ Sco (Mathias et al. 1991). A detailed NLTE abundance analysis showed a nitrogen excess of ~ 0.3 dex with respect to the average nitrogen abundance in B-type stars in the solar neighbourhood. Previous abundance studies of hot stars indicate that

the appearance of such an excess may be linked to the presence of a magnetic field (e.g., Morel et al. 2006, 2008; Przybilla & Nieva 2010).

The first spectropolarimetric observations of V1449 Aql were obtained with the multi-mode instrument FORS 1 at the VLT on two consecutive nights in 2007 and revealed a change in polarity from one night to the next and the presence of a weak magnetic field on the second night of observations (Hubrig et al. 2009). In the present work we discuss 13 new spectropolarimetric observations acquired during the last two years at the 2.56 m Nordic Optical Telescope using the SOFIN echelle spectrograph. The new longitudinal magnetic field measurements are used to determine the stellar rotation period and to put constraints on the magnetic field geometry.

2. Magnetic field measurements and period determination

Multi-epoch series of polarimetric spectra of V1449 Aql with $S/N \geq 200$ were obtained with the low-resolution camera ($R = \lambda/\Delta\lambda \approx 30\,000$) of the high-resolution echelle spectrograph SOFIN (Tuominen et al. 1999) mounted at the Cassegrain focus of the Nordic Optical Telescope (NOT) in 2009 August–September and in 2010 July. We used a 2 K Loral CCD detector to register 40 echelle orders partially covering the range from 3500 to 10 000 Å with a length of the spectral orders of

---

Table 1. Magnetic field measurements of V1449 Aql with SOFIN.

JD – 245 0000	Phase	$\langle B_z \rangle$ [G]	JD – 2 450 000	Phase	$\langle B_z \rangle$ [G]
4343.659	0.790	-55 ± 33	5397.567	0.648	-430 ± 89
4344.584	0.856	166 ± 41	5398.530	0.717	-255 ± 211
5071.396	0.171	-21 ± 95	5400.574	0.864	168 ± 168
5073.391	0.314	-380 ± 159	5402.577	0.008	421 ± 115
5076.389	0.530	-647 ± 153	5405.646	0.229	-204 ± 131
5078.429	0.677	-326 ± 171	5407.559	0.367	-416 ± 133
5080.392	0.818	-115 ± 102	5409.648	0.517	-663 ± 427
5395.564	0.504	-729 ± 232			

Notes. In the first two lines we list the earlier FORS 1 measurements published by Hubrig et al. (2009). Phases are calculated according to the ephemeris of JD = 2 455 305.21 + 13.893 E. All quoted errors are 1σ uncertainties.

Fig. 2. Phase diagram with the best sinusoidal fit for the longitudinal magnetic field measurements with a reduced $\chi^2 = 0.46$. The residuals (Observed – Calculated) are shown in *the lower panel*. The two FORS 1 measurements appear in green.
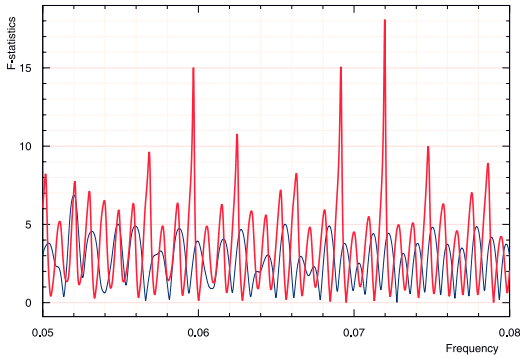

Fig. 1. The periodogram of V1449 Aql built from the longitudinal magnetic field measurements with the most prominent frequency at $f = 0.0720\,\mathrm{d}^{-1}$, corresponding to a period of 13.893 days. The lower thin line presents the window function.

about 140 Å at 5500 Å. Two exposures with the quarter-wave plate angles separated by 90° are necessary to derive circularly polarized spectra. The spectra are reduced with the 4A software package (Ilyin 2000). Wavelength shifts between the right- and left-hand side circularly polarized spectra were interpreted in terms of a longitudinal magnetic field $\langle B_z \rangle$, using the moment technique described by Mathys (1994).

The magnetic field measurements with SOFIN and FORS 1 are presented in Table 1. In the first column we list the heliocentric Julian dates for the middle of the spectropolarimetric observations. The phases of the measurements of the magnetic field are shown in Col. 2, and in Col. 3 we present the mean longitudinal magnetic field $\langle B_z \rangle$. An example of Stokes I and Stokes V profiles of N ɪɪ in the wavelength region $\lambda\lambda$ 4775–4800 is presented in Fig. A.1.

The frequency analysis was performed on the 13 SOFIN longitudinal magnetic field measurements and two previous FORS 1 measurements using a non-linear least-squares fit of the multiple harmonics utilising the Levenberg-Marquardt method (Press et al. 1992) with an optional possibility of pre-whitening the trial harmonics. To detect the most probable period, we calculated the frequency spectrum and for each trial frequency we performed a statistical F-test of the null hypothesis for the absence of periodicity (Seber 1977). The resulting periodogram displays three dominant peaks with the highest peak at $f = 0.0720\,\mathrm{d}^{-1}$ corresponding to a period $P = 13^{\mathrm{d}}.893$. In the framework of the rigid rotator model usually assumed for magnetic stars on the upper main-sequence, the period of the magnetic field variation corresponds to the stellar rotation period. In Fig. 1 we show that two lower peaks appear at $f = 0.069162\,\mathrm{d}^{-1}$ and $f = 0.059689\,\mathrm{d}^{-1}$
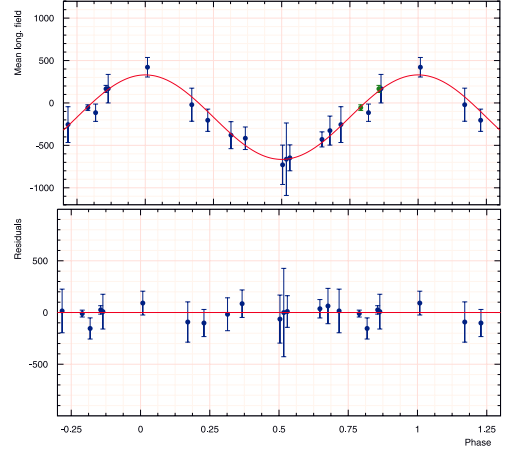
with equivalent periods of $P = 14^{\mathrm{d}}.459$ and $P = 16^{\mathrm{d}}.753$, respectively. Since two measurements in our data set were obtained with the low-resolution FORS 1 spectrograph, we carried out a few tests to evaluate the significance of these measurements for the period determination. We find that omitting the FORS 1 measurements from the period search leads to the dominance of a frequency peak corresponding to a period of $14^{\mathrm{d}}.496$. On the other hand, the period search without weighting tied to the measurement accuracies leads to a much stronger dominance of the frequency peak $f = 0.0720\,\mathrm{d}^{-1}$ with the equivalent period of $P = 13^{\mathrm{d}}.893$. The referee of this paper informed us that his implementation of a CLEAN analysis leads to a detection of the same periods, but favors the period of $P = 14^{\mathrm{d}}.459$. These results show that the periodicity determination may depend on the technique used and that the relevance of the frequencies $f = 0.069162\,\mathrm{d}^{-1}$ and $f = 0.059689\,\mathrm{d}^{-1}$ is difficult to ascertain at the present stage without additional magnetic data. The derived ephemeris for the detected period corresponding to the highest frequency peak is

$$\langle B_z \rangle^{\mathrm{pos.extr.}} = \mathrm{HJD}\ 2\,455\,305.21 \pm 0.16 + 13.893 \pm 0.003E. \quad (1)$$

The phase diagram of the magnetic field measurements for the determined period is presented in Fig. 2.

The measurements of the longitudinal magnetic field in V1449 Aql require, however, special care in treating the data, as the timescale of a complete single observation of the length of ~40 min with SOFIN, including two subexposures, is comparable to the timescale of the pulsation variability. As we mention above, two subexposures with the quarter-wave plate angles separated by 90° are needed to derive circularly polarized spectra. To remove the instrumental effects of small misalignments, differences in transmission, etc., the complete observation of a star usually consists of at least two successive subexposures with the waveplate rotated by 90° to exchange the positions of the two spectra on the CCD. The final Stokes I and V spectra are then calculated from the polarized spectra by taking the respective averages. To obtain Stokes I, the two average corresponding spectra, in our case the average of $(I + V)_0$ and $(I + V)_{90}$ are added with the average of $(I - V)_0$ and $(I - V)_{90}$, while Stokes V is calculated from the difference of the two spectra, the average of $(I+V)_0$ and $(I+V)_{90}$ and of $(I-V)_0$ and $(I-V)_{90}$. However, owing to very strong changes in the line profile positions and shapes in the strongly pulsating V1449 Aql, the method of using respective average spectra would lead to erroneous wavelength shifts
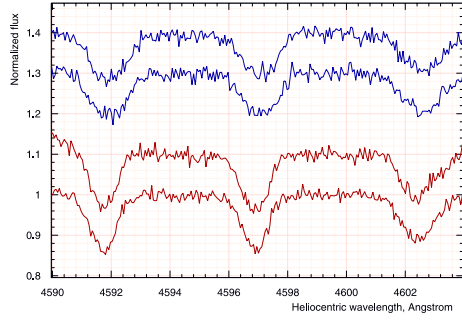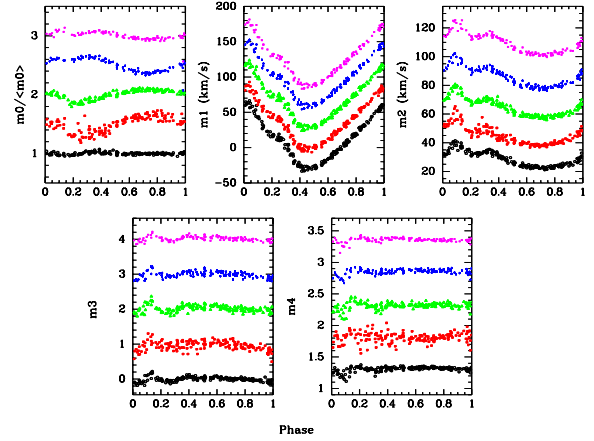
Fig. 3. Variability of the output spectra in two SOFIN subexposures taken with the quarter-wave plate angles separated by 90° taken around HJD 2 455 398.530. The lower two spectra, $(I + V)_0$ and $(I - V)_0$, correspond to the first subexposure, while the upper spectra, $(I - V)_{90}$ and $(I + V)_{90}$, correspond to the second subexposure. The strong effect of pulsations on the line profile shapes and the line positions is clearly visible between the spectra of the first subexposure with a duration of 20 min and the spectra of the second subexposure with the same duration.
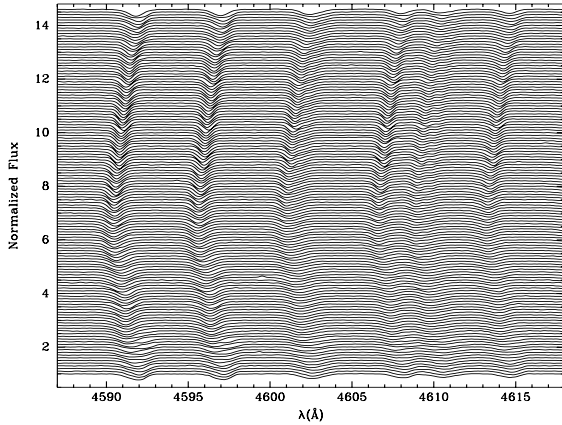
Fig. 4. Time series of FEROS spectra showing pulsational line profile variability in the spectral region 4590–4615 Å. The pulsation phase zero is at the bottom.

Fig. 5. Velocity moments of line profiles: equivalent width (m0), radial velocity (m1), line width (m2), asymmetry (m3), and kurtosis (m4). In each panel five curves are plotted corresponding to five spectral lines of various elements: He I 4713.1, C II 5133.1, N II 5667.6, O II 4592.0, and Si III 4553.6, shown *from bottom to top*.

Table 2. Magnetic field model for V1449 Aql.

$\overline{\langle B_z \rangle}$	[G]	-167.5 ± 27.3
$A_{\langle B_z \rangle}$	[G]	498.1 ± 37.1
P	[d]	13.893 ± 0.003
R	$[R_\odot]$	11.2 ± 1.4
$v_{\rm eq}$	[km s^{-1}]	41 ± 5
$v \sin i$	[km s^{-1}]	24 ± 2
i	[°]	36 ± 6
β	[°]	76 ± 4
$B_{\rm d}$	[G]	3100 ± 300

and thus to wrong values of the longitudinal magnetic field. The behaviour of all four spectra in both subexposures taken around HJD 2 455 398.530 is illustrated in Fig. 3. To remedy this situation, we decided to carry out the measurements of the line shifts between the spectra $(I + V)_0$ and $(I - V)_0$ in the first subexposure and the spectra $(I - V)_{90}$ and $(I + V)_{90}$ in the second subexposure separately. The final longitudinal magnetic field value was then calculated as an average of the measurements for each subexposure.

The line profiles undergo very significant pulsational variability, and any rotational modulation of the observed profiles is completely masked by the pulsational modulation. In Fig. A.2 we demonstrate the behaviour of the O II and He I line profiles in SOFIN spectra in the spectral region 4695–4715 Å over the rotation cycle. The inspection of 224 FEROS spectra used in the study of Briquet et al. (2009) reveals that all lines behave in a rather similar way. In Fig. 4 we present a clear pulsation pattern in the spectral region 4590–4615 Å. The moment variations for five lines belonging to different elements, namely He I 4713.1, C II 5133.1, N II 5667.6, O II 4592.0, and Si III 4553.6, shown in Fig. 5, however, exhibit slight differences between the elements. The equivalent widths of O II and Si III are larger at the phase of minimum radius, while C II and N II are larger at the maximum radius. The equivalent width of He I is almost constant. At minimum radius the elements N, C, and O show line profiles

narrower than those of Si and He. Also the amplitude of the radial velocity curve of the He I line is about 4 km s^{-1} greater than for the C II line and 2 km s^{-1} more than for the N II line.

The longitudinal field of V1449 Aql can be adequately represented by a single-wave variation curve during the stellar rotation cycle (see Fig. 2), indicating a dominant dipolar contribution to the magnetic field topology. Assuming that V1449 Aql is an oblique dipole rotator, the magnetic dipole axis tilt β is constrained by $\langle B_z \rangle^{\rm max} / \langle B_z \rangle^{\rm min} = \cos(i + \beta) / \cos(i - \beta)$. In Table 2 we show the mean value $\overline{\langle B_z \rangle}$ and the semi-amplitude of the field variation $A_{\langle B_z \rangle}$ for V1449 Aql in rows 1 and 2. Values for $v_{\rm t} = 44$ km s^{-1}, which is the total line broadening, and $v_{\rm eq} = 38 \pm 15$ km s^{-1} were published by Briquet et al. (2009). The stellar radius, $R = 11.2 \pm 1.4 R_\odot$, was calculated using main-sequence evolutionary CLÉS models (Scuflaire et al. 2008). Obviously, the accuracy of the determination of $v_{\rm eq}$ from the best-fit-solutions of the spectroscopic mode identification described in the work of Briquet et al. (2009) is rather low. However, the equatorial rotation velocity can also be calculated using the relation $v_{\rm eq} = 50.6 R/P$, where $R = 11.2 \pm 1.4 R_\odot$ is the stellar radius in solar units and $P = 13.893$ d the period in days. Using this formula, we obtain $v_{\rm eq} = 41 \pm 5$ km s^{-1}. On the other hand, Lefever (private communication) obtained $v \sin i = 24$ km s^{-1}, using the different procedure described in Lefever et al. (2010), which takes macroturbulent broadening into account. Our own estimate of the $v \sin i$ value, $v \sin i = 23.5$ km s^{-1} using the technique of Díaz et al. (2011) fully agrees with that of Lefever. The combination of $v \sin i = 24$ km s^{-1} with a typical estimation error of 2 km s^{-1} and $v_{\rm eq} = 41 \pm 5$ km s^{-1} leads to the inclination angle $i = 36 \pm 6°$. In the last two rows, we list the parameters of the magnetic field dipole model.
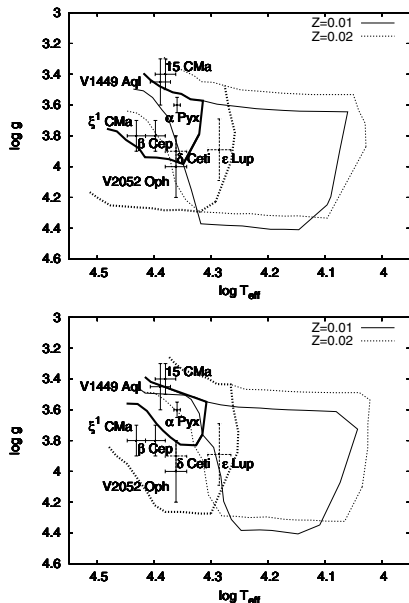
Fig. 6. The position of the β Cephei and candidate β Cephei stars in the H-R diagram. *Upper panel*: the boundaries of the theoretical instability strips are calculated using the OP opacities. *Lower panel*: boundaries are calculated using OPAL opacities. Full lines correspond to strips for metallicity $Z = 0.01$ and dotted lines to strips with metallicity $Z = 0.02$. The thick and thin lines correspond to the boundaries of the β Cephei and SPB instability regions, respectively.

3. Discussion

Using FORS 1/2 and SOFIN longitudinal magnetic field measurements collected in our recent studies, we were able to detect a weak mean longitudinal magnetic field of a few hundred Gauss in four β Cephei stars, δ Cet, ξ^1 CMa, 15 CMa, and V1449 Aql, and in two candidate β Cephei stars, α Pyx and ϵ Lup (Hubrig et al. 2006, 2009, 2011). Before we started our systematic search for magnetic fields in pulsating B-type stars, a weak magnetic field was detected in two other β Cephei stars, in the prototype of the class, β Cep itself, by Henrichs et al. (2000) and in V2052 Oph by Neiner et al. (2003). The strongest longitudinal magnetic fields were detected in the two β Cephei stars with the large radial velocity amplitudes, namely in V1449 Aql and ξ^1 CMa, for which peak-to-peak amplitudes reach $\sim$90 km s^{-1} and $\sim$33 km s^{-1}, respectively. The rather strong magnetic field in the atmosphere of these two stars and the rather low $v \sin i$ values, certainly make these stars the most suitable targets for studying the impact of magnetic fields on stellar rotation, pulsations, element diffusion, and frequency patterns.

In the frequency analysis of the CoRoT data obtained for V1449 Aql (Degroote et al. 2009), the frequency $f = 0.068790 \pm 0.000393$ d^{-1} is, within the errors, close to the frequency $f = 0.069162$ d^{-1} detected in our study of the periodicity using magnetic field measurements. Additional magnetic field measurements will be worthwhile for proving whether this photometric frequency corresponds to the rotation/magnetic period of this star.

Our studies indicate that dipole models provide a satisfactory fit to the magnetic data and among the presently known magnetic β Cephei stars, ξ^1 CMa and V1449 Aql, possess the largest magnetic fields, with a dipole strength of several kG. The position of the currently known eight magnetic β Cephei and candidate β Cephei stars in the $\log T_{\rm eff} - \log g$ diagram is presented in Fig. 6 together with the boundaries of the theoretical instability strips calculated for different metallicities ($Z = 0.01$ and $Z = 0.02$) and using the OP opacities (http://cdsweb.u-strasbg.fr/topbase/op.html, see also Miglio et al. 2007) and OPAL opacities (http://opalopacity.llnl.gov/opal.html). The stellar fundamental parameters and their literature sources are compiled in Table A.1. We give in the same table the information on the dominant mode and the radial velocity amplitude, if known. The extent and the position of the instability strip are highly dependent on the opacities used and on the metallicity adopted. Recent studies indicate, however, a lower metallicity than $Z = 0.02$ for early B-type stars in the solar neighbourhood with $Z = 0.014$ (e.g. Przybilla et al. 2008). Although the sample of magnetic pulsating stars is still very small, and it is difficult to determine any trend in the distribution of the stars in the H-R diagram, it might seem that magnetic stars are clustered rather close to the instability strip boundaries (full lines in left panel of Fig. 6). Certainly, additional future magnetic field studies of a larger sample of β Cephei stars are needed to study the indicated trend.

References

Aerts, C., de Pauw, M., & Waelkens, C. 1992, A&A, 266, 294
Aerts, C., Mathias, P., Gillet, D., & Waelkens, C. 1994, A&A, 286, 109
Belkacem, K., Samadi, R., Goupil, M.-J., et al. 2009, Science, 324, 1540
Briquet, M., Uytterhoeven, K., Morel, T., et al. 2009, A&A, 506, 269
Crowe, R., & Gillet, D. 1989, A&A, 211, 365
Degroote, P., Briquet, M., Catala, C., et al. 2009, A&A, 506, 111
Díaz, C. G., González, J. F., Levato, H., & Grosso, M. 2011, A&A, 531, A143
Henrichs, H. F., Neiner, C., Hubert, A. M., et al. 2000, ASPC, 214, 372
Heynderickx, D. 1992, A&AS, 96, 207
Heynderickx, D., Waelkens, C., & Smeyers, P. 1994, A&AS, 105, 447
Hubrig, S., Briquet, M., Schöller, M., et al. 2006, MNRAS, 369, L61
Hubrig, S., Briquet, M., De Cat, P., et al. 2009, AN, 330, 317
Hubrig, S., Ilyin, I., Schöller, M., et al. 2011, ApJ, 726, L5
Ilyin, I. 2000, Ph.D. Thesis, University of Oulu, Finland
Lefever, K., Puls, J., Morel, T., et al. 2010, A&A, 515, A74
Mathias, P., Gillet, D., & Crowe, R. 1991, A&A, 252, 245
Mathys, G. 1994, A&AS, 108, 547
Miglio, A., Montalbán, J., & Dupret, M.-A. 2007, Comm. in Asteroseismology, 151, 48
Morel, T., Butler, K., Aerts, C., et al. 2006, A&A, 457, 651
Morel, T., Hubrig, S., & Briquet, M. 2008, A&A, 481, 453
Neiner, C., Henrichs, H. F., Floquet, M., et al. 2003, A&A, 411, 565
Press, W. H., Teukolsky, S. A., Vetterling, W. T., & Flannery, B. P. 1992, Numerical Recipes, 2nd edn. (Cambridge: Cambridge University Press)
Przybilla, N., & Nieva, M. F. 2010, in Active OB stars – structure, evolution, mass loss, and critical limits, ed. C. Neiner, G. Wade, G. Meynet, & G. Peter, IAU Symp., 272, in press [arXiv:1011.5977]
Przybilla, N., Nieva, M.-F., & Butler, K. 2008, ApJ, 688, L103
Przybilla, N., Firnstein, M., Nieva, M. F., et al. 2010, A&A, 517, A38
Saesen, S., Briquet, M., & Aerts, C. 2006, Comm. in Asteroseismology, 147, 109
Scuflaire, R., Théado, S., Montalbán, J., et al. 2008, Ap&SS, 316, 83
Seber, G. A. F. 1977, Linear Regression Analysis (New York: Wiley)
Telting, J. H., Schrijvers, C., Ilyin, I. V., et al. 2006, A&A, 452, 945
Tuominen, I., Ilyin, I., & Petrov, P. 1999, in Astrophysics with the NOT, ed. H. Karttunen, & V. Piirola, University of Turku, Tuorla Observatory, 47
Waelkens, C., Aerts, C., Kestens, E., et al. 1998, A&A, 330, 215

Appendix A: Additional material

Table A.1. Fundamental parameters of β Cephei and candidate β Cephei stars with detected magnetic fields.

Object Name	T_{eff} [K]	$\log g$	Reference	Dominant mode	RV amplitude [km s^{-1}]	Reference
δ Cet	$23\,000 \pm 1000$	3.90 ± 0.10	1	$f = 6.2026\,\mathrm{d}^{-1}$	7.44	5
ξ^1 CMa	$27\,000 \pm 1000$	3.80 ± 0.10	1	$f = 4.77153\,\mathrm{d}^{-1}$	16.4	6
15 CMa	$24\,000 \pm 1000$	3.40 ± 0.10	1	$f = 5.42\,\mathrm{d}^{-1}$		7, 8
α Pyx	$22\,900 \pm 300$	3.60 ± 0.05	2	β Cep candidate		9
ϵ Lup	$19\,300 \pm 900$	3.89 ± 0.20	3	β Cep candidate		9
V2052 Oph	$23\,000 \pm 1000$	4.00 ± 0.20	1	$f = 7.148\,\mathrm{d}^{-1}$	6.7	10
V1449 Aql	$24\,500 \pm 1000$	3.45 ± 0.15	4	$f = 5.48694\,\mathrm{d}^{-1}$	44.0	4
β Cep	$25\,000 \pm 1000$	3.80 ± 0.10	1	$f = 5.250\,\mathrm{d}^{-1}$	21	11

References. 1 – Lefever et al. (2010); 2 – Przybilla et al. (2010); 3 – Hubrig et al. (2009); 4 – Briquet et al. (2009); 5 – Aerts et al. (1992); 6 – Saesen et al. (2006); 7 – Heynderickx (1992); 8 – Heynderickx et al. (1994); 9 – Telting et al. (2006); 10 – Neiner et al. (2003); and 11 – Aerts et al. (1994).
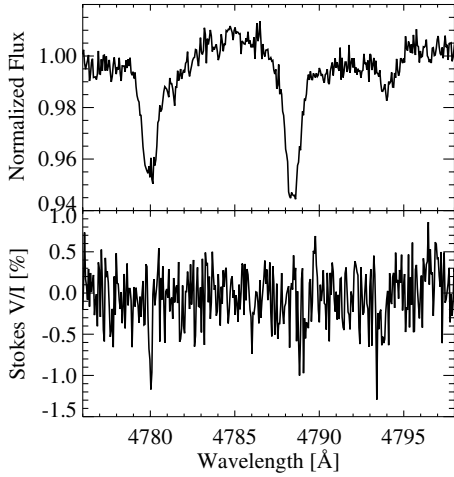
Fig. A.1. An example of Stokes I and Stokes V spectra observed at phase 0.648 in the wavelength region $\lambda\lambda$ 4775–4800 containing several N II spectral lines.
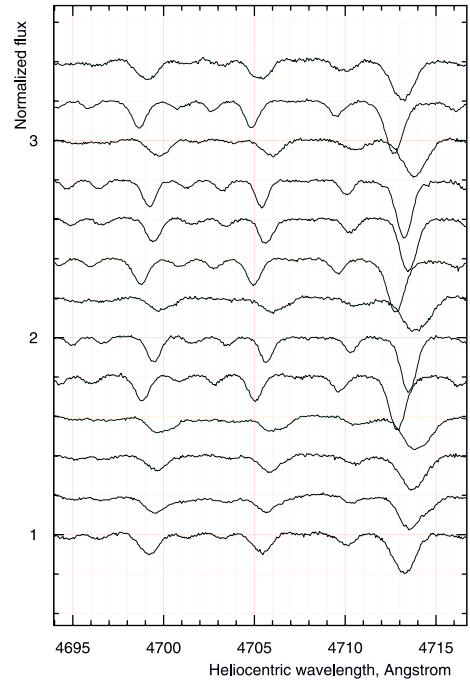
Fig. A.2. Line profile variability of O II $\lambda\lambda$4699, 4705, 4710, and He I λ4713 over the rotation cycle on SOFIN spectra. The spectra are presented with phases increasing *from bottom to top* and offset in the vertical direction for clarity.